IEEE Transactions on Nuclear Science, Vol. NS-28, No. 3, June 1981

FOUR-DIMENSIONAL BEAM TOMOGRAPHY*

G. N. Minerbo, O. R. Sander, and R. A. Jameson
Los Alamos National Laboratory, Los Alamos, NM 87545

Summary

A computer code has been developed to reconstruct the 4-D transverse phase-space distribution of an accelerator beam from a set of linear profiles measured at different angles at three or more stations along the beam line. The code was applied to wire-scan data obtained on the low-intensity H^- beam of the LAMPF accelerator. A 4-D reconstruction was obtained from 10 wire-scan profiles; 2-D projections of the reconstruction agree fairly well with slit-and-collector measurements of the horizontal and vertical emittance distributions.

Reconstruction Technique

An algorithm for reconstructing the 4-D transverse phase-space distribution

$$f\left(\begin{bmatrix} x \\ x' \\ y \\ y' \end{bmatrix}\right)$$

of a beam from a set of linear profiles was given in Ref. 1. Wire scanners or optical measurements provide samplings of J one-dimensional projections of f, denoted by

$$g_j(u_1) = \int du_2 \int du_3 \int du_4 \; f\left(T_j^{-1} \begin{bmatrix} u_1 \\ u_2 \\ u_3 \\ u_4 \end{bmatrix}\right), \quad j = 1, \ldots, J \; . \tag{1}$$

In the simplest case of interest, the transfer matrices T_j correspond to a drift followed by a rotation about the z-axis

$$T = \begin{bmatrix} \cos\theta & L\cos\theta & \sin\theta & L\sin\theta \\ 0 & \cos\theta & 0 & \sin\theta \\ -\sin\theta & -L\sin\theta & \cos\theta & L\cos\theta \\ 0 & -\sin\theta & 0 & \cos\theta \end{bmatrix} . \tag{2}$$

Thus g_j is the 1-D profile measured at an angle θ_j from the (horizontal) x-axis at a position $z = L_j$ from the origin.

The 4-D reconstruction problem is severely underdetermined; the maximum entropy approach[1] produces a solution that is the "most probable" consistent with the data for g in Eq. (1). The algorithm in Ref. 1 was first implemented using a simple trapezoidal rule to evaluate the required 3-D integrals. This version of the code was prohibitively time consuming. We describe below two improvements that decreased the execution time by about a factor of 10 for the same accuracy. First, we start the MENT iterations[1] from a 4-D Gaussian distribution whose projections have the same RMS width as the measured profiles g_j. Second, we use Gaussian quadrature rules[2,3] with the weights and abscissas of Hermite polynomials to evaluate the 3-D integrals. The variational procedure to maximize the entropy needs to be reformulated somewhat to accommodate these two changes.

*Work performed under the auspices of the US Department of Energy.

We assume, for simplicity that f has been normalized and centered as follows:

$$\int d^4v \; f(v) = 1, \quad \int d^4v \; v_n \; f(v) = 0, \quad n = 1, \ldots, 4.$$

The transfer matrices have $\det T_j = 1$ under very general conditions, hence the g_j will also be normalized and centered. We define b_j, the RMS width of g_j, by

$$b_j^2 = \int du \; u^2 \; g_j(u), \quad j = 1, \ldots, J \; . \tag{3}$$

The covariance matrix σ of f is defined as

$$\sigma_{mn} = \int d^4v \; v_m \; v_n \; f(v), \quad m,n = 1, \ldots, 4 \; . \tag{4}$$

The relation between b_j and σ is

$$b_j^2 = S_j \; \sigma \; S_j^+ \; , \tag{5}$$

where S_j is a 1 x 4 submatrix of T_j,

$$S = [T_{11} \; T_{12} \; T_{13} \; T_{14}] \; , \tag{6}$$

and S^+ denotes the transpose of S.

Since σ is symmetric, it has 10 independent elements. At least J = 10 profiles are needed to find σ. However, if the T_j have the form shown in Eq. (2), σ cannot be completely determined for any J. The matrices in Eq. (2) have the property

$$T_{11} \; T_{14} = T_{12} \; T_{13} \; ; \tag{7}$$

thus $\sigma_{14} - \sigma_{23}$ is not fixed by Eq. (5). This indeterminacy persists for any T-matrices that commute with the matrix

$$\mathcal{R} = \begin{bmatrix} 0 & 0 & 1 & 0 \\ 0 & 0 & 0 & 1 \\ -1 & 0 & 0 & 0 \\ 0 & -1 & 0 & 0 \end{bmatrix} . \tag{8}$$

$\mathcal{R}$ is the generator of rotations about the z-axis, and $\sigma_{14} - \sigma_{23}$ is proportional to the mean value of the angular momentum of the beam. If T is produced by Hamiltonian time evolution, it has the symplectic property.[4] It can be shown that, if T is symplectic and T commutes with $\mathcal{R}$, then T must satisfy Eq. (7). Placing quadrupole magnets between stations is one way of removing the indeterminacy in $\sigma_{14} - \sigma_{23}$. However solenoidal fields or space-charge forces are not effective in removing the indeterminacy.

The procedure we follow is to first find the function ϕ with the largest entropy that has the same b_j as the measured profiles. The entropy H of ϕ is defined as

$$H = - \int d^4v \; \phi(v) \; \ln \phi(v) \; . \tag{9}$$

The solution, obtained by variational techniques,[5] is

$$\phi(v) = \pi^{-2} \; (\det G)^{1/2} \; \exp[-(v, G\, v)] \; , \tag{10}$$

where the 4 x 4 matrix G has the form

$$G = \sum_j \gamma_j \; S_j^+ \; S_j \; . \tag{11}$$

0018-9499/81/0600-2231$00.75©1981 IEEE

The relation $\sigma = \frac{1}{2} G^{-1}$, used in Eq. (5), determines the γ_j.

Once ϕ is known, we reconstruct f by maximizing the conditional entropy[5] (that is, the entropy of f given ϕ)

$$H(f|\phi) = -\int d^4v\, f(v) \ln [f(v)/\phi(v)], \qquad (12)$$

with Eq. (1) treated as constraints. By using Lagrange multipliers, one finds that f must have the form

$$f(v) = \phi(v) \prod_j h_j (S_j v) \quad . \qquad (13)$$

The unknown 1-D functions h_j are determined by inserting Eq. (13) into Eq. (1)

$$g_j(u_1) = h_j^{i+1}(u_1) \int du_2 \int du_3 \int du_4\, \phi(T_j^{-1}u) \times \prod_{k\neq j} h_k^{i} (S_k T_j^{-1} u) \quad . \qquad (14)$$

The superscript i indicates the iteration number. The functions h_j are initially set to unity and updated according to Eq. (14). Because the present algorithm starts from a Gaussian distribution ϕ that matches the b_j of the input profiles, fewer iterations are needed. We found that two or three iterations will usually produce an adequate match to the data for the g_j.

To evaluate the integrals in Eq. (14) we need a quadrature rule for integrals of the form

$$I = \int du_2 \int du_3 \int du_4 \exp [(-u, Q_j u)]\, \chi(u) \quad . \qquad (15)$$

We first perform a Cholesky decomposition[6] of $Q_j = T_j^{-1+} G\, T_j^{-1}$ into factors E that are lower triangular $Q_j = E^+ E$, and compute the inverse of E, $F = E^{-1}$ which is also lower triangular. With the change of variables $w = Eu$, the integral I becomes

$$I = F_{22} F_{33} F_{44} \int dw_1 e^{-w_1^2} \int dw_2 e^{-w_2^2} \int dw_3 e^{-w_3^2} \times \int dw_4 e^{-w_4^2} \chi(Fw) \quad . \qquad (16)$$

Gaussian quadrature rules based on Hermite polynomials[2] of order N are applied successively to the three 1-D integrations in Eq. (16). Adequate accuracy is obtained with N = 11 in practical situations. The matrices E and F can be computed efficiently with subroutines SPOCO and STRDI in the LINPACK library.[6]

Experimental Reconstructions

Wire scanners at three stations separated by about 90 cm were used to obtain profiles of the LAMPF beam at 750 keV. The mechanism of the wire-scanner actuators did not allow us to obtain vertical scans ($\theta = 90°$). Instead, we used sampling angles of approximately -60°, 0°, and +60° from the horizontal. At the first station, an additional profile was obtained at about 45°. The values of L, θ, and the computed value of b for the 10 profiles are given in Table I.

As a check on the reconstruction procedure, we obtained slit-and-collector measurements of the horizontal and vertical emittance distributions near the central station. Six complete sets of data were

Table I
Geometrical Parameters of Measured Profiles

Profile j	L_j (cm)	θ_j (degrees)	b_j (cm)
1	-91.2	59.1	0.176
2	-90.9	44.8	0.183
3	-90.6	-0.5	0.200
4	-90.2	-60.0	0.158
5	-0.2	59.8	0.138
6	0	-0.3	0.131
7	0.2	-59.7	0.133
8	93.2	61.6	0.231
9	93.4	1.4	0.247
10	93.5	-59.1	0.265

obtained for different conditions of beam and detectors. All six data sets produced viable reconstructions although the accuracy of the reconstruction varied. Results obtained with the first data set are reported below. For the transfer matrices, we used the simple form in Eq. (2); space-charge corrections were not needed.

The σ matrix computed from Eqs. (5) and (11) was (in units of cm and radians)

$$\sigma = \begin{bmatrix} 1.71\text{-}2 & 5.27\text{-}5 & 7.17\text{-}4 & -1.77\text{-}5 \\ 5.27\text{-}5 & 3.98\text{-}6 & -4.38\text{-}5 & -5.26\text{-}7 \\ 7.17\text{-}4 & -4.38\text{-}5 & 1.88\text{-}2 & 1.03\text{-}4 \\ -1.77\text{-}5 & -5.26\text{-}7 & 1.03\text{-}4 & 2.71\text{-}6 \end{bmatrix} \qquad (17)$$

The cross-correlation coefficients

$$\frac{\sigma_{13}}{\sqrt{\sigma_{11}\sigma_{33}}} = 0.04, \quad \frac{\sigma_{24}}{\sqrt{\sigma_{22}\sigma_{44}}} = -0.16, \quad \frac{\sigma_{14} - \sigma_{23}}{(\det \sigma)^{1/4}} = 0.12 \qquad (18)$$

are small for this beam, but not negligible.

The 4-D reconstruction algorithm converged in two iterations and required three minutes on a CDC 7600 computer. The original version of the code typically required six iterations and a total of three hours of CDC 7600 time. Two-dimensional projections of the reconstructed 4-D distribution f are shown in Figs. 1A, 1B, and 1C. The horizontal emittance distribution

$$\Xi(x,x') = \int dy \int dy'\, f\left(\begin{bmatrix} x \\ x' \\ y \\ y' \end{bmatrix}\right) \qquad (19)$$

shown in Fig. 1A also can be reconstructed by processing profiles 3, 6, and 9 with the 2-D emittance code of Ref. 1. The results obtained with the 2-D code are displayed in Fig. 1D. Figure 1E shows the results obtained by applying the 2-D tomography code of Ref. 7 to profiles 5, 6, and 7. The agreement between the 4-D and 2-D codes was generally good. For comparison we include in Figs. 1F and 1G the slit-and-collector measurements of the horizontal and vertical emittance distribution. Figure 1A is fairly close to 1F on a quantitative basis, but the agreement between Figs. 1C and 1G is not as good. However, the vertical emittance was not optimally sampled with our choice of viewing angles.

Four-dimensional reconstruction techniques will be deployed[8] on the Hanford Fusion Materials Irradiations Test Facility (FMIT) accelerator under construction at Los Alamos. Light emitted by ionized or excited residual gases will be collected by TV cameras and digitized. The TV cameras allow flexibility in the choice of viewing angles: four views at 0°, 45°, 90°, and 135° will be obtained at each of three stations. The accuracy of the 4-D reconstructions should be improved by having 12 profiles instead of 10.

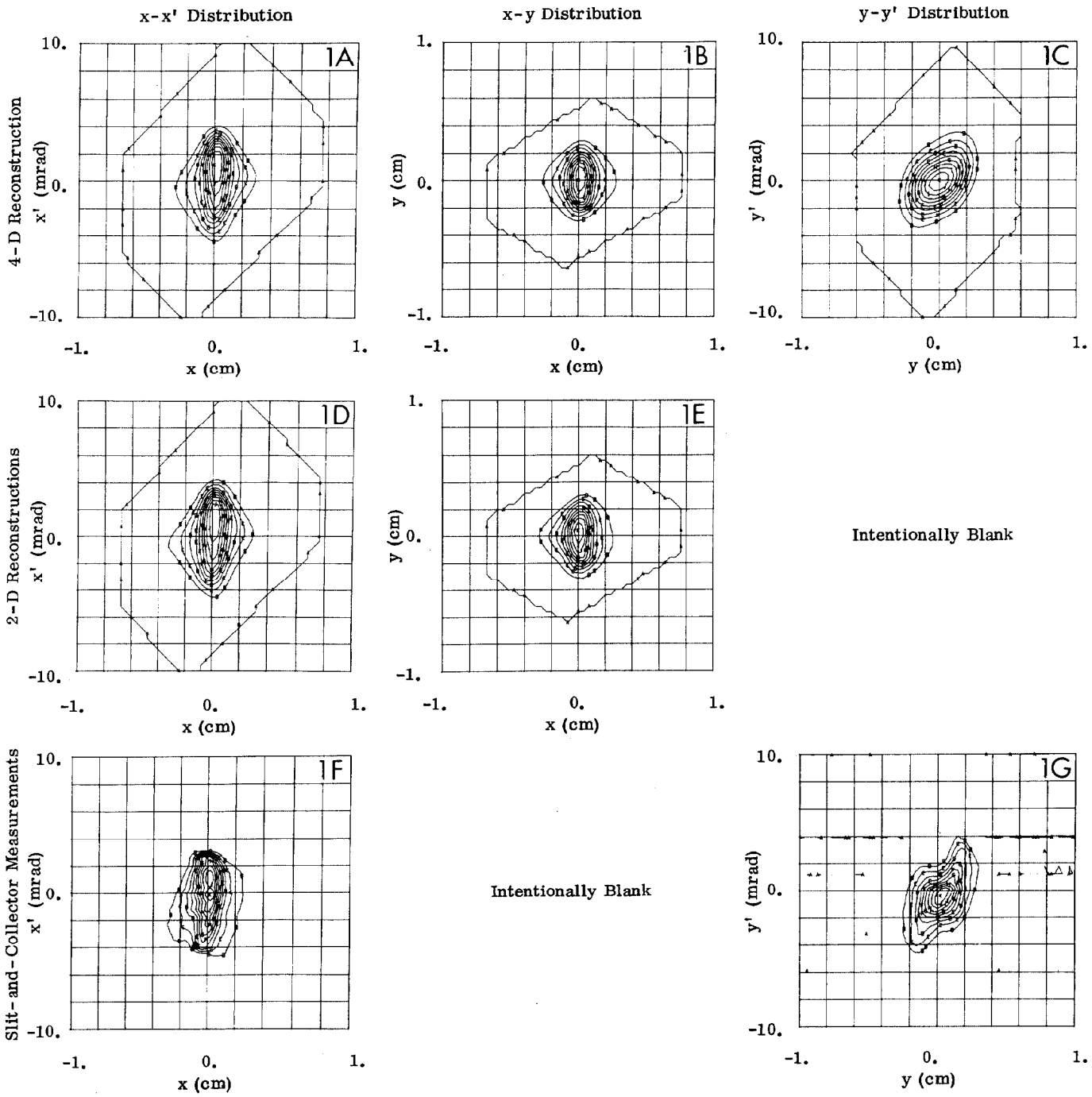

Fig. 1. Comparison of 4-D reconstruction, 2-D reconstructions, and slit-and-collector measurements. Figures 1A, 1B, and 1C are 2-D projections of the reconstructed 4-D distribution. The reconstructions in Figs. 1D and 1E were obtained with 2-D reconstruction algorithms. Figures 1F and 1G are the horizontal and vertical emittance distributions measured directly with slit-and-collector instrumentation.

References

1. O. R. Sander, G. N. Minerbo, R. A. Jameson, and D. D. Chamberlin, "Beam Tomography in Two and Four Dimensions," Proc. 1979 Linear Accelerator Conference, Montauk, NY, Sept. 10-14, 1979 (Brookhaven Nat. Lab., Upton, NY, 1980) BNL-51134, 314-318.
2. M. Abramowitz and I. A. Stegun, Handbook of Mathematical Functions, (Nat. Bureau of Standards, Washington, DC, 1964) 890, 924.
3. D. K. Kahaner, Nat. Bureau of Standards, Washington, DC, private communication, 1980.
4. E. D. Courant and H. S. Snyder, Theory of the Alternating-Gradient Synchrotron, Ann. Phys. 3, 1-48 (1958).
5. C. E. Shannon and W. Weaver, Mathematical Theory of Communication, (Univ. Illinois Press, Urbana, IL, 1962), Sec. 20.
6. J. J. Dongarra, C. B. Moler, J. R. Bunch, and G. W. Stewart, LINPACK Users' Guide, (Society for Industrial and Applied Mathematics, Philadelphia, PA, 1979), Chaps. 3,6.
7. G. Minerbo, "MENT: A Maximum Entropy Algorithm for Reconstructing a Source from Projection Data," Computer Graphics Image Processing 10, 48-68 (1979).
8. D. D. Chamberlin, G. N. Minerbo, L. E. Teel, and J. D. Gilpatrick, "Noninterceptive Transverse Beam Diagnostics," Paper E-80, this Conference.